# Type III secretion system effector protein BipC: Role in *Burkholderia pseudomallei* intracellular trafficking

Wen Tyng Kang, Kumutha Malar Vellasamy, Lakshminarayanan Rajamani, Roger W Beuerman, Jamuna Vadivelu

Melioidosis, an infection caused by the facultative intracellular pathogen *Burkholderia pseudomallei*, has been classified as an emerging disease with the number of patients steadily increasing at an alarming rate. *B. pseudomallei* possess various virulence determinants that allow them to invade the host and evade the host immune response, such as the type III secretion systems (TTSS). The products of this specialized secretion system are particularly important for the *B. pseudomallei* infection. Lacking in one or more components of the TTSS demonstrated different degrees of defects in the intracellular lifecycle of *B. pseudomallei*. Further understanding the functional roles of proteins involved in *B. pseudomallei* TTSS will enable us to dissect the enigma of *B. pseudomallei*-host cell interaction. In this study, BipC (a translocator), which was previously reported to be involved in the pathogenesis of *B. pseudomallei*, was further characterized using the bioinformatics and molecular approaches. The *bipC* gene, coding for a putative invasive protein, was first PCR amplified from *B. pseudomallei* K96243 genomic DNA and cloned into an expression vector for overexpression in *Escherichia coli*. The soluble protein was subsequently purified and assayed for actin polymerization and depolymerization. BipC was verified to subvert the host actin dynamics as demonstrated by the capability to polymerize actin *in vitro*. Homology modeling was also attempted to predict the structure of BipC. Overall, our findings identified that the protein encoded by the *bipC* gene plays a role as an effector involved in the actin binding for the intracellular trafficking of *B. pseudomallei*.

# Type III secretion system effector protein BipC: Role in *Burkholderia pseudomallei* intracellular trafficking

**Wen-Tyng Kang[1], Kumutha Malar Vellasamy[1], Lakshminarayanan Rajamani[2], Roger W Beuerman[2], Jamuna Vadivelu [1]**

[1] Department of Medical Microbiology, Faculty of Medicine, University of Malaya, Kuala Lumpur, Malaysia.

[2] Singapore Eye Research Institute (SERI), Singapore.

Corresponding Author:

Jamuna Vadivelu [1]

Department of Medical Microbiology, Faculty of Medicine, University of Malaya, 50603 Kuala Lumpur, Malaysia.

Email address: jamuna@ummc.edu.my

**Abstract**

Melioidosis, an infection caused by the facultative intracellular pathogen *Burkholderia pseudomallei*, has been classified as an emerging disease with the number of patients steadily increasing at an alarming rate. *B. pseudomallei* possess various virulence determinants that allow them to invade the host and evade the host immune response, such as the type III secretion systems (TTSS). The products of this specialized secretion system are particularly important for the *B. pseudomallei* infection. Lacking in one or more components of the TTSS demonstrated different degrees of defects in the intracellular lifecycle of *B. pseudomallei*. Further understanding the functional roles of proteins involved in *B. pseudomallei* TTSS will enable us to dissect the enigma of *B. pseudomallei*-host cell interaction. In this study, BipC (a translocator), which was previously reported to be involved in the pathogenesis of *B. pseudomallei*, was further characterized using the bioinformatics and molecular approaches. The *bipC* gene, coding for a putative invasive protein, was first PCR amplified from *B. pseudomallei* K96243 genomic DNA and cloned into an expression vector for overexpression in *Escherichia coli*. The soluble protein was subsequently purified and assayed for actin polymerization and depolymerization. BipC was verified to subvert the host actin dynamics as demonstrated by the capability to polymerize actin *in vitro*. Homology modeling was also attempted to predict the structure of BipC. Overall, our findings identified that the protein encoded by the *bipC* gene plays a role as an effector involved in the actin binding for the intracellular trafficking of *B. pseudomallei*.

## Introduction

Melioidosis, a potentially fatal disease, is a neglected tropical disease that afflicts both humans and animals. It is caused by the Gram-negative soil saprophyte, *Burkholderia pseudomallei*. It has varied clinical presentations, including asymptomatic infection, chronic pneumonia, and fulminant septic shock with abscesses in multiple internal organs (Wiersinga, Currie & Peacock, 2012). This disease is endemic across parts of tropical South East Asia and Northern Australia (Sun & Gan, 2010). Most cases of melioidosis are the result of percutaneous inoculation following exposure to the bacteria from muddy soils or surface water (Chaowagul *et al.,* 1989). The etiological agent has been classified as Tier 1 Select Agent by the United States Centers for Disease Control and Prevention (CDC) due to its high mortality rate that could be used as a potential agent for bioterrorism (Sarovich *et al.,* 2014).

Melioidosis was classified as an emerging disease with a steady increase in the number of patients over the past few years (Dance, 2002). In addition, the fulminating septicemia form of melioidosis typically has a mortality rate of greater than 90%. Previous studies have demonstrated that *B. pseudomallei* is able to survive and replicate in both the phagocytic and non-phagocytic cells (Stevens *et al.,* 2004). However, the most striking feature of this bacterium is the ability to remain latent in the host for up to 62 years and cause recrudescent infections following many years past the initial infection (Ngauy *et al.,* 2005). Among the virulence factors of *B. pseudomallei*, the long dormancy state may be attributed to the type III secretion system (TTSS), which facilitate the pathogen to survive and replicate in both phagocytic and non-phagocytic cell (Brett & Woods, 2000; Stevens *et al.,* 2002). However, the exact mechanism of this phenomenon is still yet to be discovered.

TTSS involves a cluster of genes encoding a series of proteins that has been reported to play a role in the pathogenicity of many Gram-negative bacterial pathogens (Mecsas & Strauss, 1996). These pathogenic bacteria use the TTSS to deliver virulence factors, also known as effector proteins, from the bacterial cytoplasm into the host cell interior. The effector proteins function to facilitate entry into and survival of the bacteria in the phagosome of the host cells (He, Nomura & Whittam, 2004). Recent reports have indicated that one of the protein products of TTSS3, BipC, was present in the secretome of *B. pseudomallei* laboratory culture and it was found to be immunogenic as verified by reactivity to mice anti-*B. pseudomallei* sera (Vellasamy *et al.,* 2010). Based on the previous finding, mutation in the *bipC* gene has been shown to impair the ability of *B. pseudomallei* to adhere, invade, and survive intracellularly in the epithelial cells *in vitro*. In addition, BipC is also required for full virulence in a murine model of melioidosis (Kang *et al.,* 2015).

These findings demonstrated that BipC plays a role in *B. pseudomallei* pathogenesis, however, there are many questions that exist as to how BipC functions as potential effector protein and promote cell invasion. Therefore, it is of great interest to elucidate the structure and properties of BipC in order to obtain more information about the exact roles played by this protein. This present study that combines the *in silico* and *in vitro* studies were performed to understand the structure and possible functions of the BipC protein. These efforts are important in establishing the biological role and importance of BipC in the virulence of *B. pseudomallei*.

## Materials and Methods

### Bacterial strains, plasmids, and culture conditions

The bacterial strains and plasmids used in this study are listed in Table S1. *B. pseudomallei* K96243 (Holden *et al.,* 2004) was cultured and maintained in Luria-Bertani (LB; Difco, Detroit, Michigan, USA) broth. All plasmids were propagated in *E. coli* Top10. The *E. coli* BL21 (DE3) was used for cloning and expression purposes. pET-30a(+) (Novagen, EMD Biosciences, Germany) was used as an expression vector to express the cloned *bipC* gene. Unless stated specifically otherwise, all bacterial strains used were grown at 37ºC on LB agar and broth (Difco, Detroit, Michigan, USA) containing appropriate antibiotics.

### Sequence analysis, homology modeling, and model assessment

The linear chain of BipC containing 419 residues was submitted to various sequence analysis on SWISS-PROT (Bairoch & Boeckmann, 1992), Basic Local Alignment Search tool (BLAST) (Altschul *et al.,* 1990) and Protein Data Bank (PDB) (Berman *et al.,* 2000). Type three secretion effector (TTSE) translocation signal peptide online program, such as ModLab (http://gecco.org.chemie.uni-frankfurt.de/T3SS_prediction/T3SS_prediction.html) (Lower & Schneider, 2009), T3SEdb (http://effectors.bic.nus.edu.sg/T3SEdb/predict.php) (Tay *et al.,* 2010) and Effective T3 (http://www.effectors.org/index.jsp) (Amold *et al.,* 2009) were used to predict the presence of TTSE for BipC. The domain family analysis was performed using Pfam protein families database (Finn *et al.,* 2010). Multiple sequence alignment between BipC and the templates were performed using CLUSTALW (Thompson, Higgins & Gibson, 1994). The information regarding the secondary structure of BipC was obtained from the online bioinformatics tool which known as GOR4 secondary structure prediction (http://npsa-

pbil.ibcp.fr/cgi-bin/secpred_gor4.pl) (Riedel *et al.*, 2006). Prediction of intrinsically unstructured regions of BipC was performed using PONDR (http://www.pondr.com/) (Li *et al.,* 1999). The template for structure prediction was chosen based on the result from the pDomThreader (Lobley, Sadowski & Jones*,* 2009), $(PS)^2$-v2 (Chen, Hwang & Yang*.,* 2009), and RaptorX (Kelley *et al.,* 2015) analyses. Verification of the built model was done using PROCHECK (Laskowski *et al.,* 2015).

**Cloning and expression of BipC protein**

*B. pseudomallei* K96243 was grown in LB broth overnight at 37ºC. DNA was extracted using Wizard® genomic DNA purification kit (Promega, Madison, Wisconsin, USA) according to the manufacturer's instruction. The 1260 bp fragment of the *bipC* was amplified by PCR using a pair of specific designed primers. The primers used were as follows: forward primer 5′-CCCAAAGGATCCACGAAGTCCAAGAGGTGCGT-3′ and reverse primer 5′-CCCAAAAAGCTTTCAGGTCCGCAGATTGCC-3′. *BamH*I and *EcoR*I site is underlined in the forward and reverse primer, respectively. The PCR reaction mixture (50 µl) contained 500 ng DNA, 0.2 mM dNTP, 1× *Taq* buffer with KCl, 1.0 mM $MgCl_2$, 0.2 µM of primers, and 0.25U *Taq* DNA polymerase (Invitrogen, Carlsbad, California, USA). The PCR was performed for a cycle of denaturation at 95°C for five minutes, followed by 30 cycles at 95°C for one minute, annealing at 62°C for one minute and extension at 72°C for one minute, and lastly further extension at 72°C for five minutes. Subsequently, the amplicon was purified using the QIAquick PCR Purification Kit (Qiagen, Venlo, Netherlands).

The obtained PCR fragments were cloned into pCR®2.1-TOPO (Promega, Madison, Wisconsin, USA) and subjected to sequencing (Macrogen, South Korea). The PCR product was then cloned

137 into *BamH*I and *EcoR*I sites of pET30a(+). For protein expression, the recombinant plasmid,
138 pET30a::*bipC* was transformed into *E. coli* strain BL21(DE3) and the transformants were
139 selected on LB agar containing 50 µg/ml kanamycin. A transformant was chosen and cultured in
140 LB broth containing 50 µg/ml kanamycin for overnight at 37ºC. Subsequently, the expression of
141 histidine tag BipC was induced using 1.0 mM isopropyl thiogalactoside (IPTG). Following the
142 induction period, cells were pelleted and re-suspended in 5 mL pre-cooled buffer (10 mM
143 imidazole, 50 mM Tris-HCI, pH 7.2 and 300 mM sodium chloride). The cells were then
144 sonicated and centrifuged at 4000 × g for 10 minutes.
145
146 **Purification of BipC protein**
147 The expressed protein from the cell culture supernatants was first purified by Nickel-
148 nitrilotriacetic acid (Ni-NTA) affinity chromatography using QIAexpress® Ni-NTA fast start kit
149 (Qiagen, Venlo, Netherlands) according to the manufacturer's instruction. Briefly, 250 ml
150 cultures of *E. coli* cells were disrupted by lysis with 10 ml native lysis buffer and incubated on
151 ice for 30 minutes. The cell lysate was centrifuged at 4°C to pellet the cellular debris and the
152 resulting cell supernatant was then transferred to a fast start column. The flow-through fraction
153 was collected. Next, the column was washed two times in 4 ml of native wash and eluted using
154 native elution buffer. The first purified protein was further purified using size exclusion
155 chromatography (SEC). In brief, 100 µl of BipC protein was added to a Sephadex® size
156 exclusion column (Amersham Biosciences, Buckinghamshire, UK) with 1 ml increments, at a
157 rate of 1 ml/min, for 30 minutes. The sample was allowed to settle into the bed of the column
158 and eluted with 10mM phosphate-buffered saline (PBS). Aliquots were collected at one minute
159 intervals and ultraviolet (UV) absorbance spectra of the eluents were analyzed. The purity of the

protein preparation was finally assessed by sodium dodecyl sulphate polyacrylamide gel electrophoresis (SDS-PAGE). Following reaction with size exclusion filtration as described above, the BipC fractions eluted were analyzed with high performance liquid chromatography **(**HPLC). Total soluble protein concentrations were then determined by the Bradford protein assay (Bradford, 1976).

**Far UV-Circular Dichroism (CD) spectropolarimetry of BipC**

BipC protein was prepared to a concentration of 0.05, 0.10, 0.25, and 0.50 mg/ml in 10mM phosphate buffer (pH 7.0). CD spectropolarimeter (Jasco J-810, Great Dunmow, Essex, UK) was purged with nitrogen gas for 15 minutes prior to introduction of sample. The CD spectrum was recorded in phosphate buffer solution (PBS) in the far UV region (190-260 nm) and all the scans were background subtracted with the scans of buffer alone. Thermal denaturation was performed with different temperature/wavelength (20-90$^{o}$C/222nm) to infer the thermal stability of the protein. The measurements were performed using a 0.1 cm path-length cuvette at 25$^{o}$C. Four scans were recorded for each spectrum. An average result was taken and baseline subtracted. The mean residual weight ellipticity ($\theta_{MRW}$) was calculated using the following equation:

$$[\theta]_{mrw} = ([\theta]_{obs} \times MRW) / (10 \times c \times l)$$

where $[\theta]_{obs}$ is the observed ellipticity in millidegrees, MRW is molecular weight of protein divided by the number of peptide bonds, c is the protein concentration and *l* is the optical path-length of the cuvette.

**Cytotoxicity assay of BipC**

To determine the cytotoxicity of BipC, human lung epithelial cell line A459 (ATCC® CCL-185™) was first seeded at $5 \times 10^4$ cells/well in a 96-well plate. Aliquots of BipC protein with final concentrations of 0.05-1 mg/ml in the plate were added to the cells and incubated overnight at 37ºC with 5% $CO_2$. The released cytolytic lactate dehydrogenase (LDH) was determined using the CytoTox96 kit (Promega, Madison, Wisconsin, USA) according to the manufacturer's instructions. In brief, a 100 µl aliquot of the supernatant obtained from each well was added to a 96-well plate. The LDH release (% cytotoxicity) was then calculated using the following equation: ($OD_{490}$ experimental release-$OD_{490}$ spontaneous release)/($OD_{490}$ maximum release-$OD_{409}$ spontaneous release) × 100. The spontaneous release was the amount of LDH released from the cytoplasm of uninfected cells, whereas the maximum release was the amount released by total lysis of uninfected cells using Triton X-100. The assays were performed in triplicate and repeated two times. The phenotype of A549 cells following 24 hours of post-exposure to the different concentration of BipC was observed under the microscope. The uninfected cells were served as negative control.

**Actin polymerization and depolymerization assays**

Actin polymerization assay was performed using Actin polymerization biochem Kit™ (Cytoskeleton, Inc., Denver, Colorado, USA) according to the manufacturer's instructions. In brief, stock of purified His-BipC protein (1 mg/ml) was prepared in an actin compatible buffer. For polymerization, G-actin stock (0.4 mg/ml) was prepared with G-buffer. The mixture was then incubated on ice for one hour in order to depolymerize actin oligomers that have formed during storage. Pyrene actin and unlabeled actin were mixed 1:1 and diluted to a final

concentration of 200 µg/ml in G-buffer. The mixture (200 µl) was then transferred into 96-well microtiter plates. Baseline fluorescence was monitored for five minutes at 37°C using a Fluoroscan fluorescence microtiter plate reader (Labsystems, Helsinki, Finland) with $\lambda_{excitation}$ at 355 nm and $\lambda_{emission}$ at 405 nm.

Polymerization was initiated by the addition of 10× actin polymerization buffer followed by mixing for 10 seconds. Actin polymerization, as determined by an increase in pyrene fluorescence, was monitored at various time points. For treatment with BipC, serial dilutions of BipC were prepared in $ddH_2O$ from 175 mM stock and 20 µl was added per ml pyrene actin mixture. The samples were examined over a period of one hour immediately after adding BipC protein. Controls included a similar volume of buffer (vehicle control). For depolymerization, stock of pyrene F-actin (1 mg/ml) was prepared by adding G-buffer. The G-actin was polymerized to F-actin by adding 10 µl of 10× actin polymerization buffer and incubated for one hour at room temperature. F-actin samples (200 µl/well) were aliquoted into microtiter plates, and the pyrene fluorescence was monitored for one hour. For BipC-treatment, 20 µl BipC (0-250 µg/ml) was added to each well before analysis.

**Protein pull down assay**

Protein-protein interaction of BipC was performed using Dynabeads® His-tag isolation and pull-down kit (Novagen, EMD Biosciences, Germany) according to the manufacturer's instructions. Sample of the histidine-tagged BipC, G-actin, and F-actin was prepared, 50 µl of Dynabeads® mixed with His-BipC and the mixture was incubated on a roller for five minutes at room temperature. The tube was placed on the magnet for two minutes and then the supernatant was discarded. The beads were washed four times with 300 µl wash buffer by placing the tube on a

magnet for two minutes and the supernatant was discarded. G-actin or F-actin was then added to the bead/BipC complex. The mixed sample was incubated on a roller for 30 minutes at room temperature, beads washed four times with 300 µl of wash buffer by placing the tube on a magnet for two minutes and the supernatant was discarded. To elute bound proteins, 100 µl his-elution buffer was added and the suspension was incubated on a roller for five minutes at room temperature. The beads at the tube wall were collected using a magnet and the supernatant containing the His-BipC and its interacting G-actin or F-actin protein was transferred to a clean tube.

## Results

### BipC sequence analysis

The bioinformatics tools (ModLab, T3Sedb, and Effective T3) used in this study predicted BipC as a TTSE, which is secreted directly into the cytosol of the host cell, based on the translocation signal peptide that was predicted to be present in the sequence of BipC (Table 1). The sequence analysis with a simple BLAST search against non-redundant (NR) database and Pfam software showed that BipC harbor a conserved domain of IpaC-SipC superfamily. Thus, the web server ClustalW was used for multiple alignments analysis of BipC, SipC (*Salmonella*), and IpaC (*Shigella*). In the sequence alignment, BipC showed that some of the residues were strictly conserved with SipC and IpaC (Fig. 1). ClustalW results showed a similarity between the target and the templates. SipC and IpaC harbors actin binding sequences at the C-terminal region. Thus, similar presence of highly conserved residues at the C-terminal of BipC may indicate that this protein also comprise of the actin binding sequences. This domain present at the C-terminal

region was also predicted to form the alpha helix secondary structure which is required for actin binding.

The GOR secondary structure prediction tool predicted BipC to contain approximately 70% of alpha helical conformations and 22% of random coil conformations (Fig. S1). The folded α-helix region may be crucial in the functionality of BipC. Prediction of the intrinsically unstructured regions of BipC was performed using the online program, PONDR. Using this software, the scores of higher than 0.5 is considered as disordered region and scores that are lower than 0.5 is considered as ordered. The results predicted an amphipathic structure comprising of alternative ordered and disordered regions for BipC (Fig. 2).

**Template-based homology modeling**

BipC amino acid residues were subjected to sequence analysis on BLAST search with Protein Data Bank (PDB) for a potential template for homology modeling. The results yield did not show any good E-value and only three structures were identified with the hits below E-value threshold. All the hits obtained shared low sequence identity with only approximately 30% within a small coverage in the sequence. Since there were no potential structural template, the web servers' pDomThreader, $(PS)^2$-v2 and RaptorX were therefore used for protein fold recognition in order to further identify the potential template for structural modeling.

From pDomThreader analysis, 1wp1B01 was identified as the best template with a high confidence level. 1wp1B01 is an X-ray structure of the outer membrane protein from *Pseudomonas aeruginosa* with the length of 405 amino acid residues and was selected as the template for model building. On the other hands, $(PS)^2$-v2 analysis identified 1tr2B as the best template with the coverage of 92.6% of the whole sequence length. 1tr2B is an X-ray structure of

a 1066 amino acid human full-length vinculin. However, the best template selected from RaptorX is 3dyjA. This structure is a 332 amino acid talin-1 from mus musculus. These templates obtained from both $(PS)^2$-v2 and RaptorX indicated that BipC shared structural features with actin binding domain, whereas template obtained from pDomThreader determined that BipC shared structural features with the transporter domain. Three of the 1wp1B01, 1tr2B, and 3dyjA were selected as the template for model building. The built models were then validated and the result indicated ~99% of the total residues fell within the most favorable and additional allowed regions for the model built using 1wp1B01 template (Fig. S2). In the 3 dimensional (3D) homology model of BipC, abundant of alpha helix regions were displayed (Fig. 3). Coupled with the Ramachandran plot, this model can be accepted as the best potential model representing the 3D structure of BipC protein.

**Cloning, expression, and purification of BipC**

A 1260 bp open reading frame (ORF) of *bipC* gene was amplified from *B*. *pseudomallei* K96243 genomic DNA (Fig. 4, lane 1) by PCR and it was cloned into a pET30a(+) vector for the expression of BipC as a 6× histidine tagged ($His_6$-tagged) protein in *E. coli*. Approximatly 90% of the $His_6$-tagged BipC was present as soluble fraction following the Ni-NTA purification. The Ni-NTA purified protein was further purified using Sephadex® size exclusion column. Here is shown the first effort to purify the protein sample in order to determine the structure of BipC (Fig. 4, lane 2). Size exclusion was successfully removed the excess molecules from the Ni-NTA purified BipC. This method of purification allowed us to obtain approximately 95% pure protein through SDS-PAGE analysis. Float-A-Lyzer dialysis device was then used for desalting of the fraction collected prior to CD analysis.

297 **Circular dichroism (CD) of purified BipC**

298 Far-UV CD spectrum was observed for BipC to determine the secondary structure of the protein.
299 The appearance of intense negative minimum around 207 and 222 nm as well as a positive
300 maximum around 195 nm confirmed the existence of a dominant α-helical structure (Fig. 5A). In
301 order to determine the thermal stability, viable temperature CD was recorded for BipC. The
302 temperature scan indicated the absence of a sharp transition even above 90°C, indicating
303 excellent thermal stability of the protein under physiological conditions (Fig. 5B).

304

305 **Cytotoxicity of BipC protein**

306 In order to identify the cytotoxic effect of BipC, A549 cells were incubated with purified His-
307 tagged BipC. A concentration-dependent increase in the LDH activity was observed after 24
308 hours of exposure. At the lowest concentration tested (5 μg/ml), about 4.5% of the LDH release
309 was observed. Release of LDH was found to increase proportionally with the increase in the
310 concentration of BipC protein exposed to the A549 cells. The highest level of LDH release
311 (51%) was observed upon exposure to 1 mg/ml of the purified BipC protein. The induction of
312 cell death was observed as compared with the untreated cells (Fig. 6A) and this data indicated
313 that the BipC may trigger the cell death to the human lung epithelial cell lines.
314 In addition, the phenotype of the A549 cells exposed to the different concentration of purified
315 His-BipC was observed using inverted microscopy (Fig. 6B). The control cells (without exposure
316 to BipC) demonstrated approximately 90% high confluency (Fig. 6B, panel i). However, the
317 A549 cells that were exposed to BipC demonstrated decreased confluency with the increasing
318 concentration of BipC. At the higher concentration of BipC (500-1000 μg/ml), the cells gradually

319 became irregular, shrunken, and detached from the cell culture substratum (Fig. 6B, panels ii, iii
320 and iv). These changes were characteristic of cell death.
321
322 **Actin polymerization and depolymerization of purified BipC *in vitro***
323 Pyrene-actin polymerization assay was performed in order to determine the involvement of BipC
324 in the assembly of actin filaments. In this assay, fluorescence of pyrene-actin increased
325 significantly when G-actin monomers were incorporated into a filament, permitting
326 polymerization to be measured in real-time. His-BipC stimulated actin polymerization in the
327 reactions containing 2 μM actin (5% pyrene-labeled) with a dose-dependent manner (Fig. 7A).
328 Saturation occurred at approximately 62.5 ug/ml of BipC and this concentration showed about 3-
329 fold increase for the actin polymerization. The data obtained with this *in vitro* actin
330 polymerization assays demonstrated that BipC has the ability to enhance actin polymerization
331 without the requirement of additional proteins.
332 Besides that, the effect of BipC on F-actin depolymerization kinetics was also monitored in this
333 study. In the presence of BipC, the percentage of pyrene-labeled F-actin was constant over 60
334 minutes, in comparison with the control (only F-actin) where only 30% remained (Fig. 7B).
335 BipC inhibited the rate of F-actin depolymerization and hence, greatly increased the stability of
336 F-actin. F-actin stabilization by higher concentration of BipC was greater than that induced by
337 the lower concentration. Taken together, these results suggest that the purified full-length BipC
338 was able to bind F-actin and modulated actin dynamics *in vitro*.
339
340
341

342 **Protein-protein interaction between BipC and actins**

343 Protein-protein interaction was performed to confirm the binding between BipC and G-actin or
344 F-actin. Both of the G- and F-actin were incubated with Dynabeads beads preloaded with His-
345 BipC. The protein pull-down assay demonstrated an interaction between these two proteins
346 where the actin binding domain was able to associate with the monomeric and filamentous actin.
347 Total molecular weight obtained for the His-BipC (~55 kDa) and F-actin (~43 kDa) was
348 approximately 98 kDa (Fig. 8, lane3). Polymerization of globular actin (G-actin) leading to a
349 structural filament (F-actin) was shown in the SDS-PAGE (Fig. 8, lane 4). This result strongly
350 suggests a role of BipC in the nucleation of actin and to promote actin bundling which is crucial
351 in *B. pseudomallei* entry into host cell membrane.

352

353 **Discussion**

354 In this study, bioinformatics analyses were exploited in order to gain preliminary insights into
355 the structural properties of BipC protein. According to Sun and Gan (2010), BipC, which plays a
356 role as a translocator protein may also play a role as an effector. Thus, the TTSEs bioinformatics
357 tools were used to determine the role of BipC as an effector. The major features used for the
358 TTSE translocation peptide prediction include the amino acid composition and positions,
359 structural properties, and physiochemical properties (Tay *et al.,* 2010; Wang *et al.,* 2013). BipC
360 harbor an N-terminal sequence that adequately fits the profile predicted by the secretion signal
361 hypothesis. Presence of signal peptide encoded in the amino acid sequence at the N-terminal of
362 BipC protein by some of the TTSE translocation peptide tools, demonstrated that this protein as a
363 pathogenicity island effector.

Interestingly, bioinformatics analysis of the entire BipC sequence identified a putative actin binding domain with sequence homology to the experimentally characterized IpaC_SipC family domain. Previous reports have indicated that IpaC and SipC harbors one actin binding domain (Chatterjee *et al.,* 2013; Knodler, Celli & Finlay*,* 2001). SipC was determined as one of the effectors with proven actin modulatory domains that nucleates and bundles actin through its N- and C-terminal domains, respectively (Hayward & Koronakis, 1999). The amino acid residues 221-260 and 381-409 of SipC were shown to bind directly to and bundles F-actin (Myeni and Zhou, 2010). Besides that, the C-terminal region of SipC was also required for the secretion and translocation of effectors into host cells (Chang, Chen & Zhao, 2005). This dual functionality of SipC provides a strong evidence showing that the functional complementation between effector domains (Hayward & Koronakis, 1999). In contrast, the SipC homologue IpaC from *Shigella* possesses the C-terminal actin nucleation domain (345-363), but with the absences of the N-terminal bundling domain (Terry *et al.,* 2008). However, the N-terminus of this protein harbors sequences for the TTSS export and interaction with IpaB and IpgC. The central hydrophobic region is mainly involved in IpaB binding, invasion, and protein stabilization (Kueltzo *et al.,* 2003; Picking *et al.,* 2001). The predicted result of ordered/disordered regions of BipC showed the amino acid sequence 140-240 of BipC falls into both the IpaC_SipC superfamily domain region and the ordered region, and therefore could be used for further structural study.

Recombinant *bipC* was expressed and purified to further understand the functional roles of this protein at the molecular level. Prior to purification through SEC, there were multiple peaks observed on the SDS-PAGE of the Ni-NTA purified BipC. Size exclusion was then performed and successfully removed the excess molecules from the Ni-NTA purified BipC. As a result, the

purified BipC protein with a high purity of approximately 95% was obtained through the SDS-PAGE analysis. Subsequently, CD spectropolarimetry was performed for the rapid determination of the secondary structure of BipC and to ensure that this protein was folded correctly. Samples for CD spectroscopy must be at least 95% pure by the criteria of HPLC, mass spectroscopy or gel electrophoresis. The CD spectra of the sample tested displayed a strong negative maxima around 197-200 nm region, suggesting that this protein possesses a well-defined alpha helix conformation. Notably, the CD spectra may change as a function of temperature, thus, leading to shifts in the baseline (Miller *et al.,* 1987). Relative change due to influence of viable temperature was monitored in this study. A sharp transition from the native state to the denatured state was observed when the protein solution was gradually heated above a critical temperature. The transition midpoint was also determined from the graph and this indicated that the purified protein was folded. Coupled with the bioinformatics online tool, the secondary structure content of the molecule was comparable with the estimated alpha-helical conformation from the CD data.

The primary sequence of BipC contains a central alpha helix region and a C-terminal alanine-rich region. A comparison between the sequences of this protein demonstrated that BipC has sequence identity with SipC and IpaC at the carboxy-terminal region. This protein also harbors a distinct F-actin binding domain, explaining the ability of BipC to assemble actin filaments, as its homolog *Salmonella* SipC and *Shigella* IpaC. Tarp effector, a multifunctional protein, which primes the host cell for bacterial entry and survival intracellularly, was shown to harbor G-actin binding or nucleating domain and two distinct F-actin binding or bundling domains (Jiwani *et al.,* 2013). These three domains mediate a direct link to the host cytoskeleton with the present of discrete sites that are specifically associated with globular or filamentous actin. In contrast, F-

actin-specific binding sites were also found in BipC, however, no typical actin-binding motifs such as the G-actin binding or nucleating domain is present in BipC. The absence of either of these actin-binding motifs raises the possibility of a novel molecular mechanism of actin assembly.

Previous studies on the bacterial effectors that influence host cell actin dynamics have provided valuable information to enhance the knowledge on the virulence factors targeting actin and contribute to a broader comprehension of actin dynamics in the eukaryotic cell (McGhie, Hayward & Koronakis, 2001; Lee, Park & Park, 2014). Thus, biophysical analysis was performed to further elucidate the functions of BipC protein in *B. pseudomallei* pathogenesis. In our previous knockout studies, BipC was shown to play a role in the actin-tail formation (Kang *et al.,* 2015). The cell attachment, movement of cells, phagocytosis, intercellular replication, and the distribution of organelles are mostly depending on the presence of the actin (Taylor, Koyuncu & Enquist, 2011). In order to achieve these processes, bacteria secrete and inject effectors to hijack the host cell machinery. The actin cytoskeleton is one of the main targets of bacterial proteins and plays a key role in the host-pathogen interaction. Hence, the interaction and binding specificity of BipC especially with actin was further investigated via protein-protein interaction and functional *in vitro* assays.

In the *in vitro* actin polymerization and protein-protein interaction studies, BipC was shown to polymerize the monomeric actin and bind independently to the F-actin. This is in agreement with previous studies that have proven the contact-dependent secretion systems such as, TTSS to be involved in actin polymerization in various other intracellular pathogens including *S. flexneri* and *S. typhimurium* (Costa *et al.,* 2015). Previous studies have shown that the N-terminus of *Salmonella* SipC protein mediates F-actin bundling activity while the C-terminal region

433 facilitates the actin nucleation activity (Hayward & Koronakis, 1999; Chang, Chen & Zhao,
434 2005; Chang *et al.,* 2007). By analogy with the SipC protein, there is a high possibility of the
435 BipC to have a similar actin nucleation and F-actin bundling activity.
436 In addition, BipC was found to bind F-actin and inhibit actin depolymerization *in vitro* without
437 the aid of a bacterial or eukaryotic factor. Contrary to BipC, the pathogenic bacterium
438 *Salmonella* SipC interacts with cellular actin and modulates its dynamics with the presence of the
439 SipA (Hayward & Koronakis, 1999; Zhao *et al.,* 1999). A study by McGhie *et al.* (2001)
440 determined that SipC-SipA collaboration generates stable networks of F-actin bundle. Unlike
441 *Salmonella* SipC, binding of F-actin by the BipC results in identifiable consequences whereby it
442 could stabilize F-actin by blocking spontaneous depolymerization in order to enhance the
443 bundling ability of the host cell actin-binding protein. Thus, it is tempting to speculate that the
444 ability of BipC in actin bundling may differ from the other intracellular pathogens.
445 The stable networks of F-actin bundles generated by BipC enhance the modulations of the
446 eukaryotic cell cytoskeleton which is essential for pathogen internalization. Actin binding
447 proteins (ABPs) present in the mammalian cells plays an important role in the remodeling of
448 cellular actin filament network, which lead to the nucleation of actin polymerization or
449 destabilization of F-actin to endorse the spatial control of filament assembly or
450 disassembly(Ayscough, 1998). Furthermore, the cellular ABPs bundle has the ability to stabilize
451 F-actin in order to generate higher order supramolecular structures that sustain membrane
452 deformations (Chen, Kaniga & Galan, 1996; Persson *et al.,* 1997; Tran Van Nhieu, Ben-Ze'ev &
453 Sansonetti, 1997). Although BipC share no primary sequence similarity to the known eukaryotic
454 ABPs, this protein was shown to bind directly to the actin and independently influences filament

dynamics. Hence, this could be the 'add on' benefit for BipC as compared to other effector proteins.

Coupled with the biophysical study, our finding indicated that BipC may play a role in the host actin dynamic. The conserved ordered region could interact with or aid in the rearrangement of highly organized cortical actin polymer networks. BipC may be able to interfere with the host cell cytoskeletal network and recruit clathrin to the site of pseudopodia engulfment in order to assist *B. pseudomallei* in the cell-to-cell entry as reported in the study on *S. flexneri* (Menard, Dehio & Sansonetti, 1996). The ability of BipC to bind actin was associated with the presence of the actin-rich regions that play a role in modulating the organelle trafficking. Overall, our findings provide a crucial insight into a novel activity of BipC protein as an effector involved in the actin binding for the intracellular trafficking of *B. pseudomallei*. The architecture of BipC-mediated actin bundles has not been studied, and hence, it will be intriguing to analyze the structure of actin bundles formed for the purpose of host-cell infection in the near future.

**Acknowledgements**

We are very grateful to Eunice Goh Tze Leng and Nandhu Muruganandham from Singapore Eyes Research Institute (SERI) for their technical assistance in the CD handling and biophysical study.

## References


1. Altschul SF, Gish W, Miller W, Myers EW, Lipman DJ. 1990. Basic local alignment search tool. *Journal of Molecular Biology* **215:** 403-410.
2. Amold R, Brandmaier S, Kleine F, Tischler P, Heinz E, Behrens S, Niinikoski A. Mewes HW, Horn M, Rattei T. 2009. Sequence-based prediction of type III secreted proteins. *PLoS Pathogens* **5:** e1000376.
3. Ayscough KR. 1998. *In vivo* functions of actin-binding proteins. *Current Opinion in Cell Biology* **10:** 102-111.
4. Bairoch A, Boeckmann B. 1992. The SWISS-PROT protein sequence data bank. *Nucleic Acids Research* **20:** 2019-2022.
5. Berman HM, Westbrook J, Feng Z, Gilliland G, Bhat TN, Weissig H, Shindyalov IN, Bourne PE. 2000. The Protein Data Bank. *Nucleic Acids Research* **28:** 235-242.
6. Bradford MM. 1976. Rapid and sensitive method for the quantitation of microgram quantities of protein utilizing the principle of protein-dye binding. *Analytical Biochemistry* **72:** 248-254.
7. Brett PJ, Woods DE. 2000. Pathogenesis of and immunity to melioidosis. *Acta Tropica* **74:** 201-210.
8. Chang J, Chen J, Zhou D. 2005. Delineation and characterization of the actin nucleation and effector translocation activities of *Salmonella* SipC. *Molecular Microbiology* **55:** 1379-1389.
9. Chang J, Myeni SK, Lin TL, Wu CC, Staiger CJ, Zhou D. 2007. SipC multimerization promotes actin nucleation and contributes to *Salmonella*-induced inflammation. *Molecular Microbiology* **66:** 1548-1556.

10. Chaowagul W, White NJ, Dance DA, Wattanagoon Y, Naigowit P, Davis TM, Looareesuwan S, Pitakwatchara N. 1989. Melioidosis: a major cause of community-acquired septicemia in northeastern Thailand. *Journal of Infectious Diseases* **159:** 890-899.

11. Chatterjee S, Chaudhury S, McShan AC, Kaur K, De Guzman RN. 2013. Structure and biophysics of type III secretion in bacteria. *Biochemistry* **52:** 2508-2517.

12. Chen CC, Hwang JK, Yang JM. 2009. $(PS)^2$-v2: template-based protein structure prediction server. *BMC Bioinformatics* **10:** 366.

13. Chen LM, Kaniga K, Galan JE. 1996. *Salmonella spp*. are cytotoxic for cultured macrophages. *Molecular Microbiology* **21:** 1101-1115.

14. Costa TRD, Felisberto-Rodrigues C, Meir A, Prevost MS, Redzej A, Trokter M, Waksman G. 2015. Secretion systems in Gram-negative bacteria: structural and mechanistic insights. *Nature Reviews in Microbiology* **13:** 343-359.

15. Dance DA. 2002. Melioidosis. *Current Opinion in Infectious Diseases* **15:** 127-132.

16. Finn RD, Mistry J, Tate J, Coggill P, Heger A, Pollington JE, Gavin OL, Gunasekaran P, Ceric G, Forslund K, Holm L, Sonnhammer EL, Eddy SR, Bateman A. 2010. The Pfam protein families database. *Nucleic Acids Research* **38:** D211-22.

17. Hayward RD, Koronakis V. 1999. Direct nucleation and bundling of actin by the SipC protein of invasive *Salmonella. EMBO Journal* **18:** 4926-4934.

18. He SY, Nomura K, Whittam TS. 2004. Type III protein secretion mechanism in mammalian and plant pathogens. *Biochimica et Biophysica Acta* **1694:** 181-206.

19. Holden MT, Titball RW, Peacock SJ, Cerdeno-Tarraga AM, Atkins T, Crossman LC, Pitt T, Churcher C, Mungall K, Bentley SD, Sebaihia M, Thomson NR, Bason N, Beacham IR, Brooks K, Brown KA, Brown NF, Challis GL, Cherevach I, Chillingworth T, Cronin

524 A, Crossett B, Davis P, DeShazer D, Feltwell T, Fraser A, Hance Z, Hauser H, Holroyd
525 S, Jagels K, Keith KE, Maddison M, Moule S, Price C, Quail MA, Rabbinowitsch
526 E, Rutherford K, Sanders M, Simmonds M, Songsivilai S, Stevens K, Tumapa S,
527 Vesaratchavest M, Whitehead S, Yeats C, Barrell BG, Oyston PC, Parkhill J. 2004. Genomic
528 plasticity of the causative agent of melioidosis, *Burkholderia pseudomallei*. *Proceedings of*
529 *the National Academy of Sciences USA*. **101:** 14240-14245.
530 20. Jiwani S, Alvarado S, Ohr RJ, Romero A, Nguyen B, Jewett TJ. 2013. *Chlamydia*
531 *trachomatis* Tarp harbors distinct G and F actin binding domains that bundle actin filaments.
532 *Journal of Bacteriology* **195:** 708-716.
533 21. Kang WT, Vellasamy K.M, Chua EG, Vadivelu J. 2015. Functional characterizations of
534 effector protein BipC, a type III secretion system protein, in *Burkholderia pseudomallei*
535 pathogenesis. *Journal of Infectious Diseases* **211:** 827-834.
536 22. Kelley LA, Mezulis S, Yates C.M, Wass MN, Sternberg MJ. 2015. The Phyre2 web portal
537 for protein modeling, prediction and analysis. *Nature Protocols* **10:** 845-858.
538 23. Knodler LA, Celli J, Finlay BB. 2001. Pathogenic trickery: deception of host cell processes.
539 *Nature Reviews Molecular Cell Biology* **2:** 578-588.
540 24. Kueltzo LA, Osiecki J, Barker J, Picking WL, Ersoy B, Picking WD, Middaugh CR. 2003.
541 Structure-function analysis of invasion plasmid antigen C (IpaC) from *Shigella flexneri*.
542 *Journal of Biological Chemistry* **278:** 2792-2798.
543 25. Laskowski RA, Macarthur MW, Moss DS, Thornton JM. 1993. Procheck - a program to
544 check the stereochemical quality of protein structures. *Journal of Applied*
545 *Crystallography* **26:** 283-291.

546 26. Lee JH, Park HJ, Park YH. 2014. Molecular mechanism of host cytoskeletal rearrangements
547 by *Shigella* invasins. *International Journal of Molecular Science*. **15**: 18253-18266.
548 27. Li X, Romero P, Rani M, Dunker AK, Obradovic Z. 1999. Predicting protein disorder for N-,
549 C-, and internal regions. *Genome Informatics Ser Workshop Genome Informatics* **10:** 30-40.
550 28. Lobley A, Sadowski MI, Jones DT. 2009. pGenTHREADER and pDomTHREADER: New
551 methods for improved protein fold recognition and superfamily discrimination.
552 *Bioinformatics* **25:** 1761-1767.
553 29. Lower M, Schneider G. 2009. Prediction of type III secretion signals in genomes of gram-
554 negative bacteria. *PLoS One* **4:** e5917.
555 30. McGhie EJ, Hayward RD, Koronakis V. 2001. Cooperation between actin-binding proteins
556 of invasive *Salmonella*: SipA potentiates SipC nucleation and bundling of actin. *EMBO*
557 *Journal.* **20:** 2131-2139.
558 31. Mecsas JJ, Strauss EJ. 1996. Molecular mechanisms of bacterial virulence: type III secretion
559 and pathogenicity islands. *Emerging Infectious Diseases* **2:** 271-288.
560 32. Menard R, Dehio C, Sansonetti PJ. 1996. Bacterial entry into epithelial cells: the paradigm of
561 *Shigella*. *Trends Microbiology* **4:** 220-226.
562 33. Miller S, Janin J, Lesk AM, Chothia C. 1987. Interior and surface of monomeric proteins.
563 *Journal of Molecular Biology*. **196:** 641-656.
564 34. Myeni SK, Zhou D. 2010. The C terminus of SipC binds and bundles F-actin to promote
565 *Salmonella* invasion. *Journal of Biological Chemistry* **285:** 13357-13363.
566 35. Ngauy V, Lemeshev Y, Sadkowski L, Crawford G. 2005. Cutaneous melioidosis in a man
567 who was taken as a prisoner of war by the Japanese during world war II. *Journal of Clinical*
568 *Microbiology* **43:** 970-972.

569 36. Persson C, Carballeira N, Wolf-Watz H, Fallman M. 1997. The PTPase YopH inhibits uptake
570 of *Yersinia*, tyrosine phosphorylation of p130Cas and FAK, and the associated accumulation
571 of these proteins in peripheral focal adhesions. *EMBO Journal* **16:** 2307-2318.
572 37. Picking WL, Coye L, Osiecki JC, Barnoski Serfis A, Schaper E, Picking WD. 2001.
573 Identification of functional regions within invasion plasmid antigen C (IpaC) of *Shigella*
574 *flexneri*. *Molecular Microbiology* **39:** 100-111.
575 38. Riedel K, Carranza P, Gehrig P, Potthast F, Eberl L. 2006. Towards the proteome of
576 *Burkholderia cenocepacia* H111: setting up a 2-DE reference map. *Proteomics* **6:** 207-216.
577 39. Sarovich DS, Price EP, Webb JR, Ward LM, Voutsinos MY, Tuanyok A, Mayo M, Kaestli
578 M, Currie BJ. 2014. Variable virulence factors in *Burkholderia pseudomallei* (melioidosis)
579 associated with human disease. *PLoS One* **9:** e91682.
580 40. Stevens MP, Haque A, Atkins T, Hill J, Wood MW, Easton A, Nelson M, Underwood-
581 Fowler C, Titball RW, Bancroft GJ, Galyov EE. 2004. Attenuated virulence and protective
582 efficacy of a *Burkholderia pseudomallei bsa* type III secretion mutant in murine models of
583 melioidosis. *Microbiology* **150:** 2669-2676.
584 41. Stevens MP, Wood MW, Taylor LA, Monaghan P, Hawes P, Jones PW, Wallis TS, Galyov
585 EE. 2002. An Inv/Mxi-Spa-like type III protein secretion system in *Burkholderia*
586 *pseudomallei* modulates intracellular behaviour of the pathogen. *Molecular Microbiology* **46:**
587 649-659.
588 42. Sun GW, Gan YH. 2010. Unraveling type III secretion systems in the highly versatile
589 *Burkholderia pseudomallei*. *Trends in Microbiology* **18:** 561-568.

590 43. Tay DM, Govindarajan KR, Khan AM, Ong TY, Samad HM, Soh WW, Tong M, Zhang F,
591 Tan TW. 2010. T3SEdb: data warehousing of virulence effectors secreted by the bacterial
592 Type III Secretion System. *BMC Bioinformatics*. **11:** S4.
593 44. Taylor MP, Koyuncu OO, Enquist LW. 2011. Subversion of the actin cytoskeleton during
594 viral infection. *Nature Review in Microbiology* **9:** 427-439.
595 45. Terry CM, Picking WL, Birket SE, Flentie K, Hoffman BM, Barker JR, Picking WD. 2008.
596 The C-terminus of IpaC is required for effector activities related to *Shigella* invasion of host
597 cells. *Microbioal Pathogenesis* **45:** 282-289.
598 46. Thompson JD, Higgins DG, Gibson TJ. 1994. CLUSTAL W: improving the sensitivity of
599 progressive multiple sequence alignment through sequence weighting, position-specific gap
600 penalties and weight matrix choice. *Nucleic Acids Research* **22:** 4673-4680.
601 47. Tran Van Nhieu G, Ben-Ze'ev A, Sansonetti PJ. 1997. Modulation of bacterial entry into
602 epithelial cells by association between vinculin and the *Shigella* IpaA invasin. *EMBO*
603 *Journal* **16:** 2717-2729.
604 48. Vellasamy KM, Mariappan V, Hashim OH, Vadivelu J. 2010. Identification of
605 immunoreactive secretory proteins from the stationary phase culture of *Burkholderia*
606 *pseudomallei*. *Electrophoresis* **32:** 310-320.
607 49. Wang G, Chen H, Zhang H, Song Y, Chen W. 2013. The secretion of an intrinsically
608 disordered protein with different secretion signals in *Bacillus subtilis*. *Current Microbiology*
609 **66:** 566-572.
610 50. Wiersinga WJ, Currie BJ, Peacock SJ. 2012. Melioidosis. *New England Journal of Medicine*
611 **367:** 1035-1044.

612 51. Zhou D, Mooseker MS, Galan JE. 1999. Role of the *S. typhimurium* actin-binding protein
613 SipA in bacterial internalization. *Science* **283:** 2092-2095.

614

# 1

Alignment of the sequences of BipC protein from *B. pseudomallei* with the SipC protein from *Samonella* and IpaC protein from *Shigella*.

The secondary structure of BipC is shown on top of the aligned sequences. Positions for which the percentage of 'equivalent' residues, considering their physico-chemical properties, is higher than 70% are colored in red on a white background. Strictly conserved residues are colored in white characters on a red background.

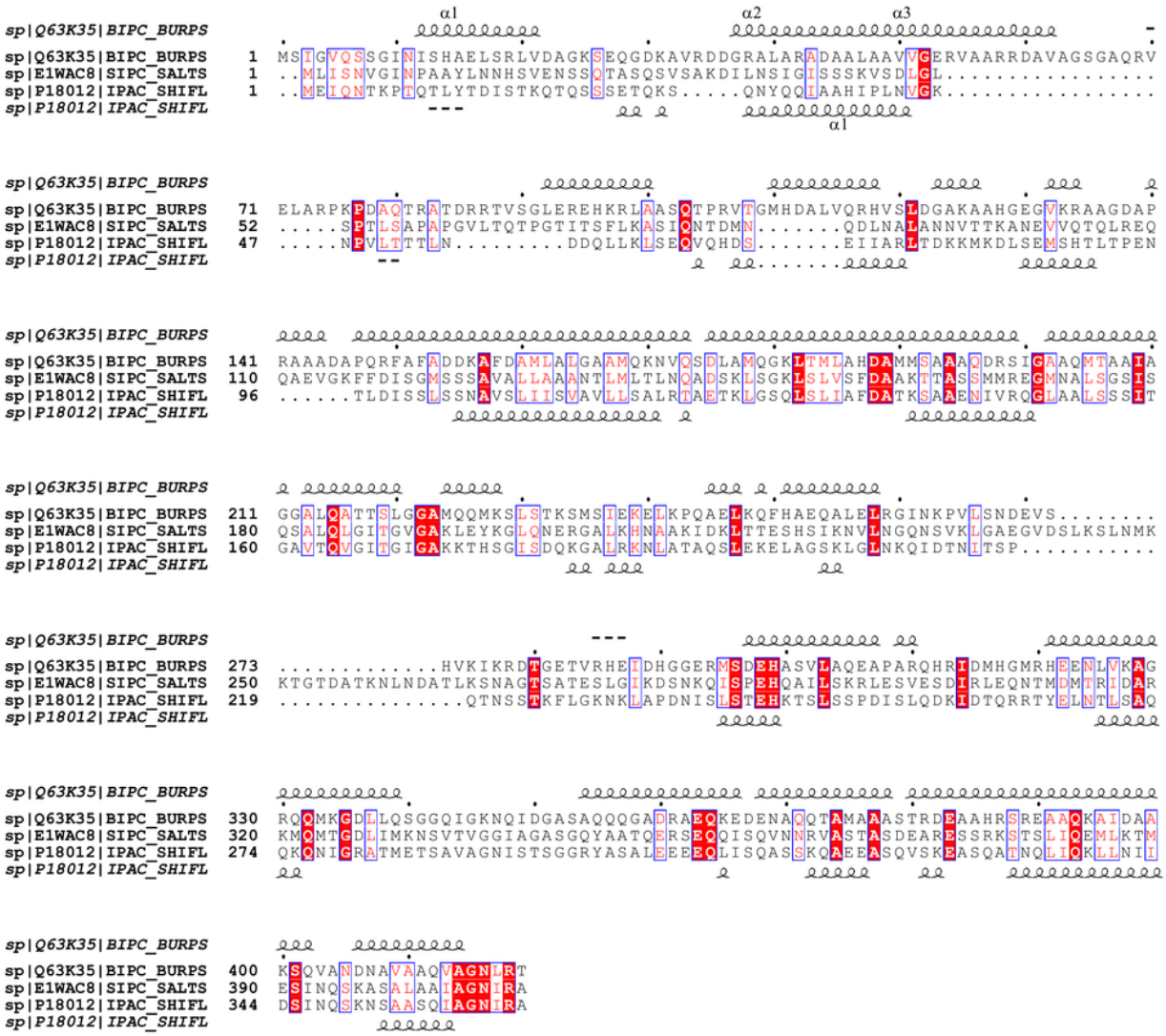

## Figure 2(on next page)

Prediction of ordered/disordered regions of BipC using PONDR.

The x-axis represents residue number and the y-axis represents PONDR score.

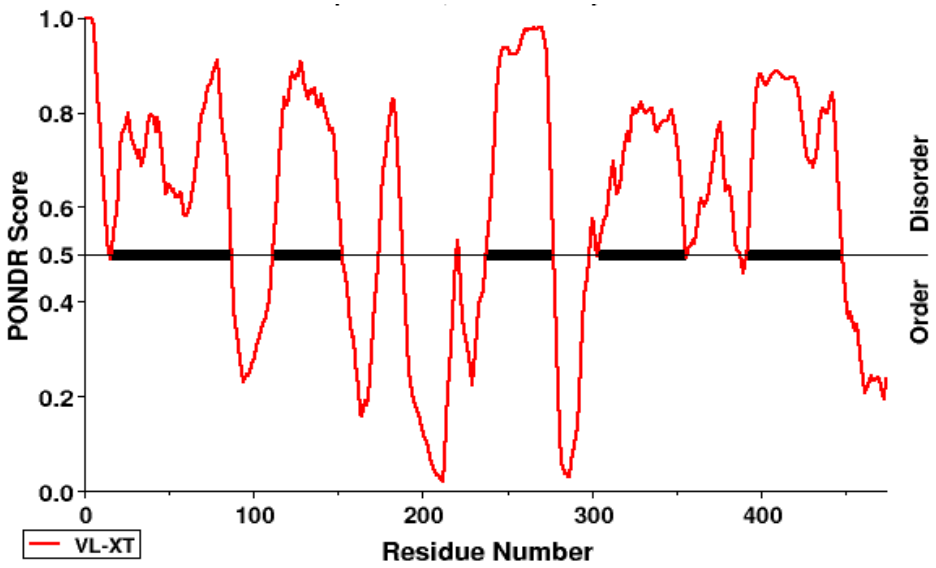
1.0
0.8
0.6
0.5
0.4
0.2
0.0
PONDR Score
Disorder
Order
0
100
200
300
400
Residue Number
VL-XT

# 3

The predicted BipC model using 1wp1B01 as a template for homology modeling with the best scoring from Ramachandran plot.

Alpha helix secondary structures are represented in purple. The graphic was generated using Visual Molecular Dynamics visualization tool.

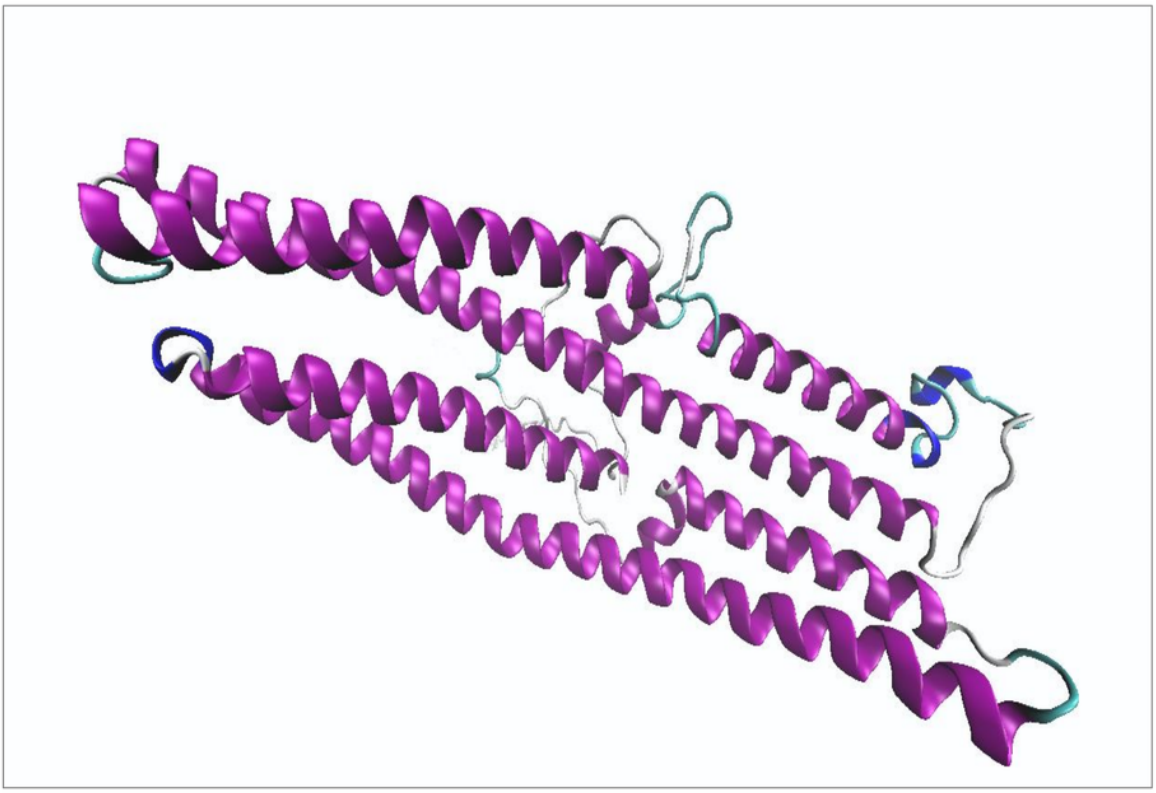

## Figure 4(on next page)

PCR amplification and expression of BipC.

(A) A 1260 bp PCR product was amplified from genomic DNA (lane 1). The PCR product from lane 1 was purified and cloned into a pET30a(+) vector for protein expression. (B) Purification of fusion protein His-BipC using Ni-NTA affinity chromatography and size exclusion chromatography. Lane M1, GeneRuler 1 kbp DNA ladder; lane 1, 1260 bp amplified *bipC*; lane M2, protein molecular weight markers; lane 2, purifiedBipC protein on 12% SDS-PAGE.

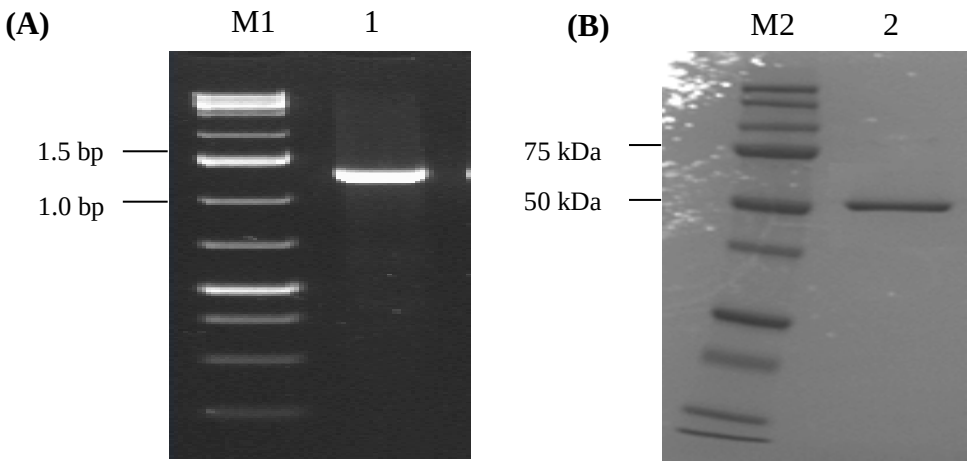
(A)
M1
1
1.5 bp
1.0 bp
(B)
M2
2
75 kDa
50 kDa

## Figure 5(on next page)

Circular dichroism spectropolarimetry of the His-BipC protein.

(A) Circular dichroism spectra of BipC in 10 mM PB, pH 7.2 at 25°C. (B) Changes of BipC protein complexes as a function of temperature used to determine the thermodynamics of folding. The viable temperature of BipC confirming the preponderance of random coil confirmation in the structure. The protein was diluted to a concentration of 0.50 mg/ml in 10 mM phosphate buffer (pH 7.2) to record the spectrum.

**(A)**

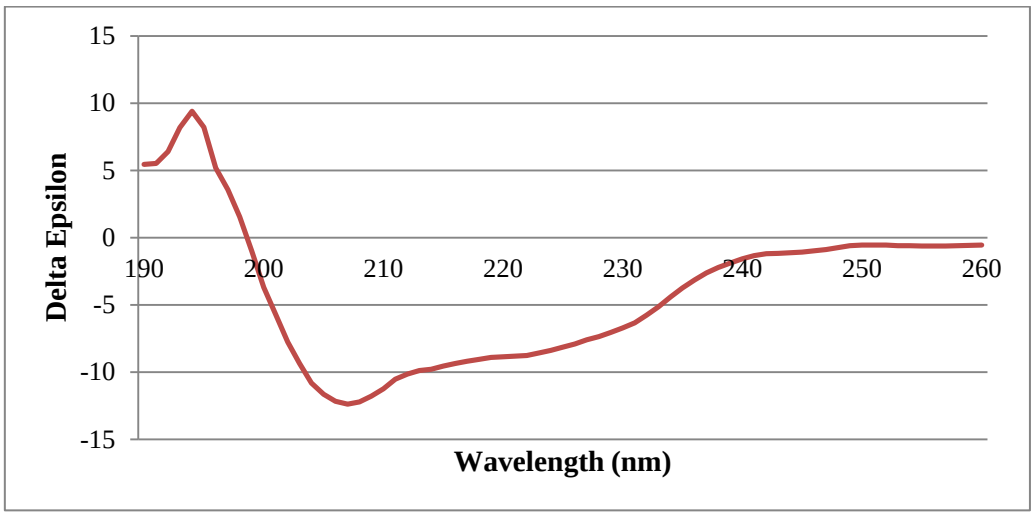
15
10
5
0
-5
-10
-15
190
200
210
220
230
240
250
260
Delta Epsilon
Wavelength (nm)

**(B)**

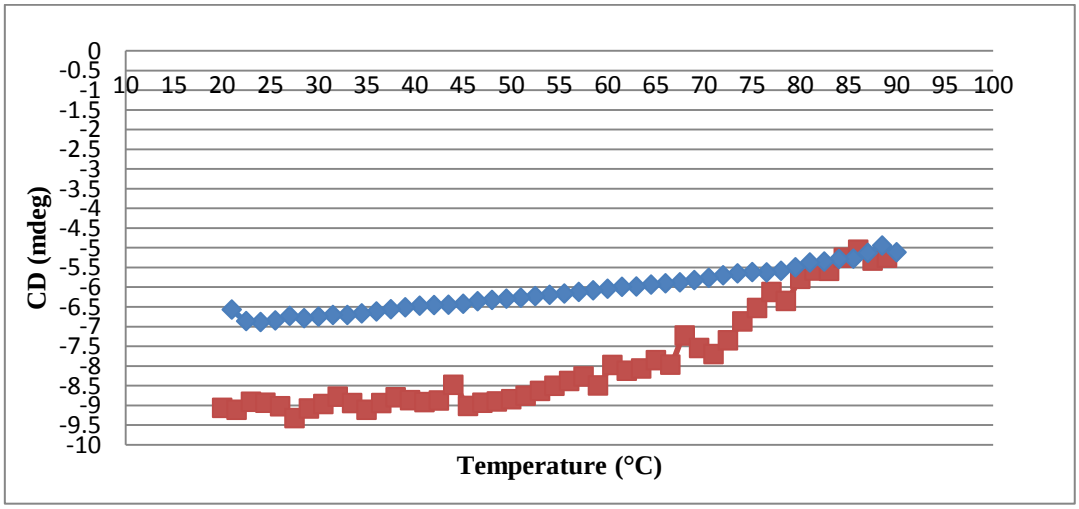
0
-0.5
-1
-1.5
-2
-2.5
-3
-3.5
-4
-4.5
-5
-5.5
-6
-6.5
-7
-7.5
-8
-8.5
-9
-9.5
-10
10 15 20 25 30 35 40 45 50 55 60 65 70 75 80 85 90 95 100
CD (mdeg)
Temperature (°C)

## Figure 6(on next page)

Cytotoxicity of BipC.

(A) Percentage of Lactate dehydrogenase (LDH) released was assayed in order to determine the cytotoxicty in A549 human lung epithelial cells exposed to BipC. The percentage of LDH released is directly proportional to the concentration of BipC. (B) A549 epithelial cells exposed to (ii) 50 µg/ml, (iii) 500 µg/ml, (iv) 1000 µg/ml of purified BipC, and (i) untreated cells (control) viewed under the light microscope.

**(A)**

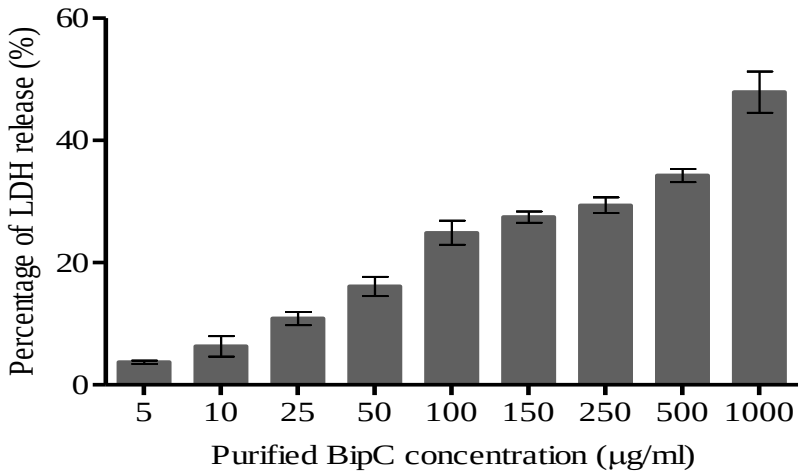
Percentage of LDH release (%)
60
40
20
0
5
10
25
50
100
150
250
500
1000
Purified BipC concentration (µg/ml)

**(B)**

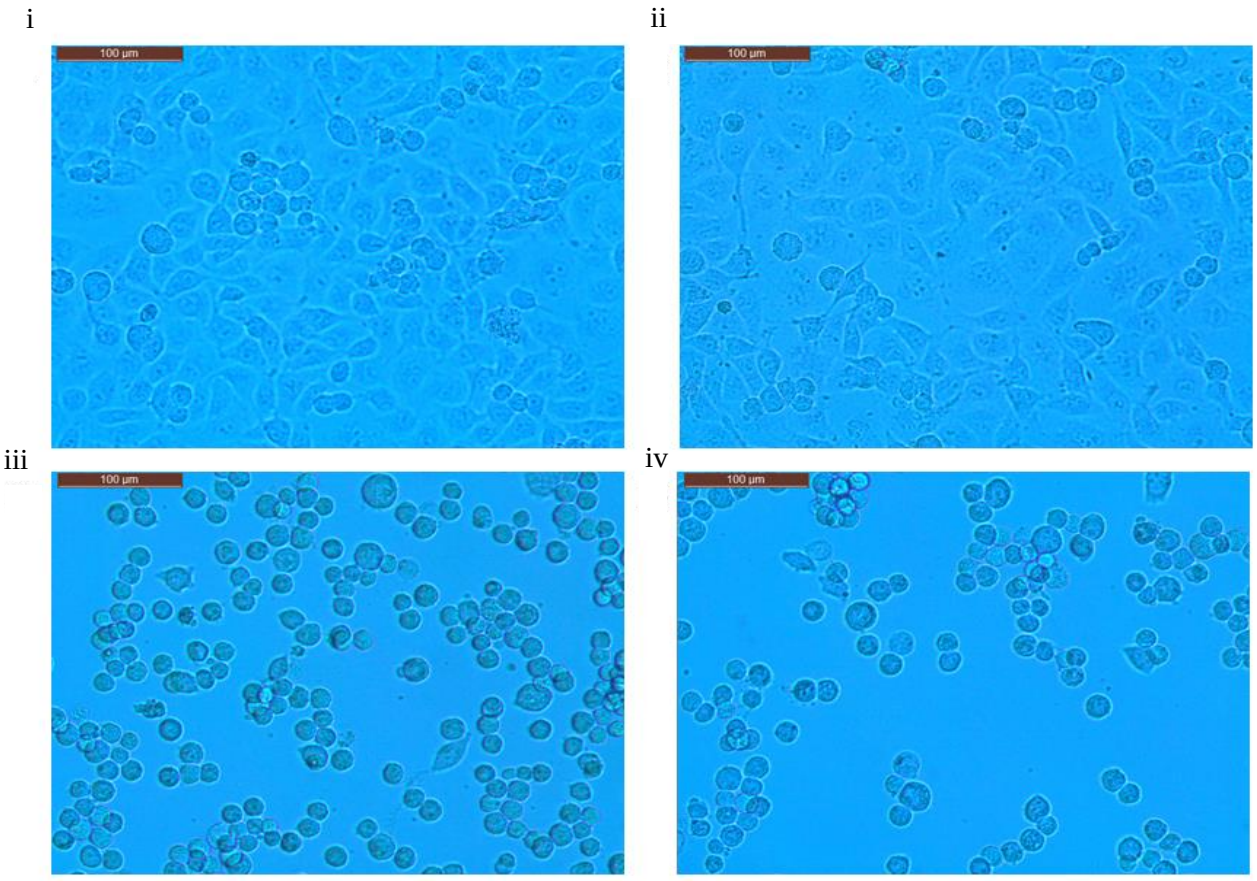
i
ii
iii
iv
100 µm

## Figure 7 (on next page)

Effect of BipC-mediated nucleation of actin polymerization and depolymerization.

Samples containing 2 mM monomeric actin (10% Pyrene-actin) and fluorescence (expressed in Arbitrary Units, AU) was measured over time after initiation of polymerisation by His-BipC. (A) Actin polymerization of His-BipC at different concentrations and (B) actin depolymerization. Velocities were determined for the interval 600-1200 seconds using the results of two independent experiments.

**(A)**

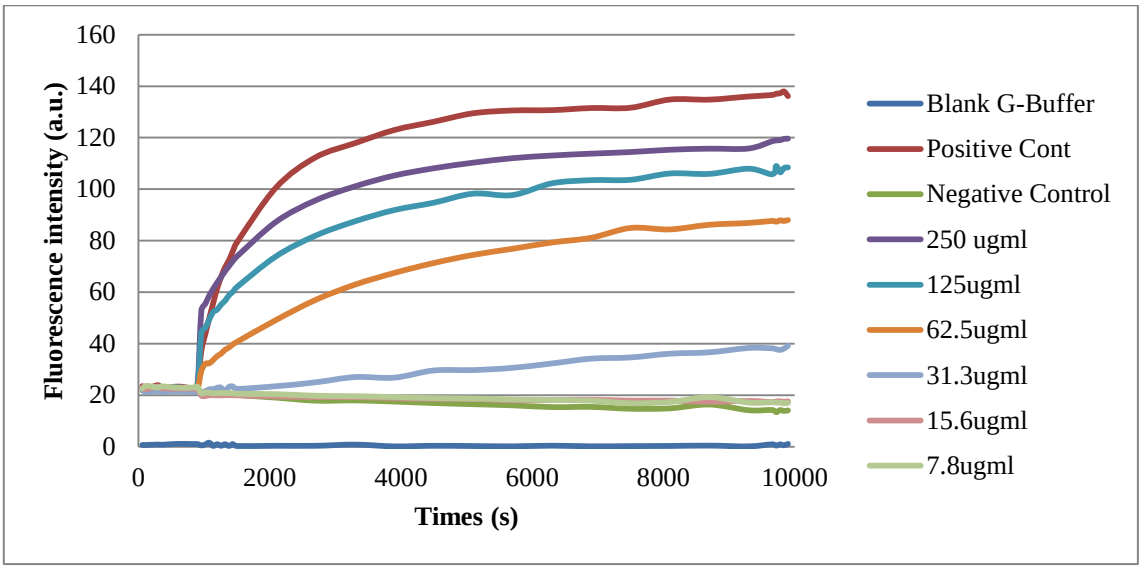
Fluorescence intensity (a.u.)
160
140
120
100
80
60
40
20
0
0
2000
4000
6000
8000
10000
Times (s)
Blank G-Buffer
Positive Cont
Negative Control
250 ugml
125ugml
62.5ugml
31.3ugml
15.6ugml
7.8ugml

**(B)**

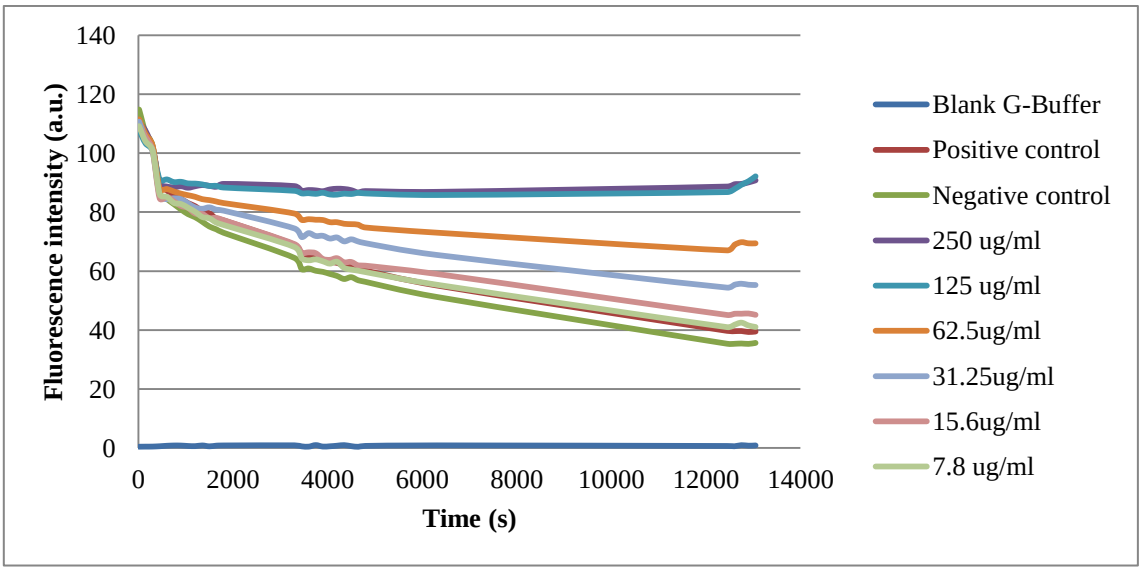
Fluorescence intensity (a.u.)
140
120
100
80
60
40
20
0
0
2000
4000
6000
8000
10000
12000
14000
Time (s)
Blank G-Buffer
Positive control
Negative control
250 ug/ml
125 ug/ml
62.5ug/ml
31.25ug/ml
15.6ug/ml
7.8 ug/ml

## Figure 8(on next page)

*In vitro* interaction analysis between His-BipC, G-actin and F-actin by pull-down assays.

This protein pull-down assay demonstrated an interaction between BipC and both of the G- and F-actin. Lane M, protein ladder; lane 1, F-actin; lane 2, His-BipC; lane 3, F-actin + His-BipC; lane 4, G-actin + His-BipC.

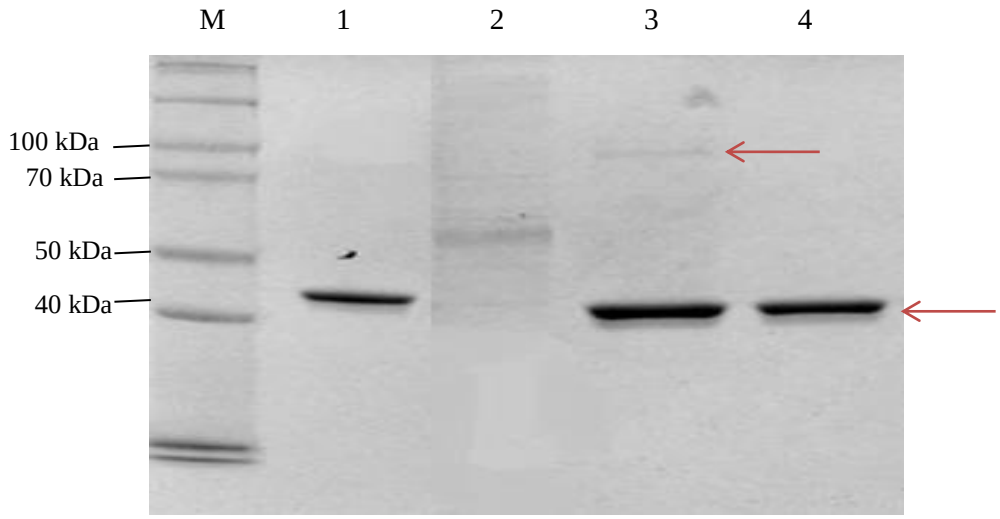
M
1
2
3
4
100 kDa
70 kDa
50 kDa
40 kDa

## Table 1(on next page)

Summary of TTSE signals peptide prediction results.

1 **Table 1. Summary of TTSE signals peptide prediction results.**

| Program | Cut off Score | Score | Prediction |
|---|---|---|---|
| ModLab | 0.400 | 1.05000 | Yes |
| T3SEdb | ≈1.000 | 1.00000 | Yes |
| Effective T3 | 0.999 | 0.52961 | Yes |

2

3